

Atomic transitions of Rb, D_2 line in strong magnetic fields: hyperfine Paschen-Back regime

A. Sargsyan¹, A. Tonoyan^{1,2}, G. Hakhumyan¹, C. Leroy², Y. Pashayan-Leroy², D. Sarkisyan¹

¹*Institute for Physical Research, 0203, Ashtarak-2, Armenia*

²*Laboratoire Interdisciplinaire Carnot de Bourgogne, UMR CNRS 6303, Université de Bourgogne, 21078 Dijon Cedex, France*

Abstract

An efficient $\lambda/2$ -method (λ is the resonant wavelength of laser radiation) based on nanometric-thickness cell filled with rubidium is implemented to study the splitting of hyperfine transitions of ^{85}Rb and ^{87}Rb D_2 lines in an external magnetic field in the range of $B = 3 \text{ kG} - 7 \text{ kG}$. It is experimentally demonstrated that at $B > 3 \text{ kG}$ from 38 (22) Zeeman transitions allowed at low B -field in ^{85}Rb (^{87}Rb) spectra in the case of σ^+ polarized laser radiation there remain only 12 (8) which is caused by decoupling of the total electronic momentum \mathbf{J} and the nuclear spin momentum \mathbf{I} (hyperfine Paschen-Back regime). Note that at $B > 4.5 \text{ kG}$ in the absorption spectrum these 20 atomic transitions are regrouped in two completely separate groups of 10 atomic transitions each. Their frequency positions and fixed (within each group) frequency slopes, as well as the probability characteristics are determined. A unique behavior of the atomic transitions of ^{85}Rb and ^{87}Rb labeled 19 and 20 (for low magnetic field they could be presented as transitions $F_g = 3, m_F = +3 \rightarrow F_e = 4, m_F = +4$ and $F_g = 2, m_F = +2 \rightarrow F_e = 3, m_F = +3$, correspondingly) is stressed. The experiment agrees well with the theory. Comparison of the behavior of atomic transitions for D_2 line compared with that of D_1 line is presented. Possible applications are described.

1. Introduction

It is well known that in an external magnetic field B the energy levels of atoms undergo splitting into a large number of Zeeman sublevels which are strongly frequency shifted, and simultaneously, there are changes in the atomic transition probabilities [1, 2]. Since cesium and rubidium are widely used for investigation of optical and magneto-optical processes in atomic vapors as well as for cooling of atoms, for Bose-Einstein condensation, and in a number of other problems [3, 4], therefore, a detailed knowledge of the behavior of atomic levels in external magnetic fields is of a high interest. The implementation of recently developed technique based on narrowband laser diodes, strong permanent magnets and nanometric-thickness cell (NTC) makes the study of the behavior of atomic transitions in an external strong magnetic field simple and robust, and allows one to study the behavior of any individual atomic transition of ^{85}Rb and ^{87}Rb

atoms for D_1 line [5, 6].

Recently, a number of new applications based on thin atomic vapor cells placed in a strong magnetic field have been demonstrated: i) development of a frequency reference based on permanent magnets and micro- and nano-cells widely tunable over the range of several gigahertz by simple displacement of the magnet; ii) optical magnetometers with micro- and/or nano-metric spatial resolution [5, 6]; iii) a light, compact optical isolator using an atomic Rb vapor in the hyperfine Paschen-Back regime is presented in [7, 8]; iv) it is demonstrated that the use of Faraday rotation signal provides a simple way to measure the atomic refractive index [9]; v) widely tunable narrow optical resonances which are convenient for a frequency locking of diode-laser radiation [10].

Strong permanent magnets produce non-homogeneous magnetic fields. In spite of the strong inhomogeneity of the B -field (in our case it can reach 15 mT/mm), the variation of B inside the atomic vapor column is by several orders less than the applied B value because of a small thickness of the cells. In case of micrometer thin cells with the thickness L in the range of 10 – 50 μm the spectral resolution is limited by the absorption Doppler line-width of an individual atomic transition (hundreds of megahertz). If the frequency distances between Zeeman sublevels are small a big number of atomic transitions are strongly overlapped and it makes absorption spectra very complicated. Fortunately, as demonstrated for Cs D_2 line, at strong ($B > 4$ kG) magnetic fields 16 atomic transitions in the absorption spectrum (there are 54 atomic transitions in moderate magnetic fields for circular polarization of the excitation field) are frequency separated from each other by a value slightly larger than the absorption Doppler line-width of an individual atomic transition [11]. That's why in this case even the use of micrometer thin cells allows one to separate practically all 16 atomic transitions (so called hyperfine Paschen-Back regime (HPB)).

Note that even for such large values as $B > 4$ kG, the atomic transitions of ^{87}Rb and ^{85}Rb D_2 lines are strongly overlapped, so pure isotope ^{87}Rb and 1 mm-atomic vapor cell have been used to separate eight Zeeman transitions [7, 8, 9]. However with this technique even in the case of using pure isotope ^{85}Rb , the atomic lines will be strongly overlapped.

Although, the HPB regime was discovered many decades earlier (see Refs. in [2, 12, 13]), however the implementation of recently developed setup based on narrowband laser diodes, strong permanent magnets and NTC makes these studies simple and robust, and allows one to study the behavior of any individual atomic transition of ^{85}Rb and ^{87}Rb atoms; the simplicity of the system also makes it possible to use it for a number of applications.

In this paper we present (for the first time to our best knowledge), the results of experimental and theoretical studies of the Rb D_2 line transitions (both ^{87}Rb and ^{85}Rb are presented) in a wide range of magnetic fields, namely for $3 \text{ kG} < B < 7 \text{ kG}$. It is experimentally demonstrated that in the case of $B > 4.5$ kG and σ^+ polarized laser radiation, there remain only 20 Zeeman transitions. In the absorption spectrum these 20 transitions are regrouped in two separate groups each of 10 atomic transitions (HPB regime), while there

are 60 allowed Zeeman transitions at low B -field.

2. EXPERIMENTAL DETAILS

2.1. Nanometric-thin cell construction

The design of a nanometric-thin cell NTC is similar to that of extremely thin cell described earlier [14]. The modification implemented in the present work is as follows. The rectangular 20 mm \times 30 mm, 2.5 mm-thick window wafers polished to < 1 nm surface roughness are fabricated from commercial sapphire (Al_2O_3), which is chemically resistant to hot vapors (up to 1000 °C) of alkali metals. The wafers are cut across the c -axis to minimize the birefringence. In order to exploit variable vapor column thickness, the cell is vertically wedged by placing a 1.5 μm -thick platinum spacer strip between the windows at the bottom side prior to gluing. The NTC is filled with a natural rubidium (72.2% ^{85}Rb and 27.8% ^{87}Rb). A thermocouple is attached to the sapphire side arm at the boundary of metallic Rb to measure the temperature, which determines the vapor pressure. The side arm temperature in present experiment was 120 °C, while the windows temperature was kept some 20 °C higher to prevent condensation. This temperature regime corresponds to the Rb atomic number density $N = 2 \cdot 10^{13} \text{ cm}^{-3}$. The NTC operated with a special oven with two optical outlets. The oven (with the NTC fixed inside) was rigidly attached to a translation stage for smooth vertical movement to adjust the needed vapor column thickness without variation of thermal conditions. Note, that all experimental results have been obtained with Rb vapor column thickness $L = \lambda/2 = 390 \text{ nm}$. For more details see [15].

2.2. Experimental setup

Figure 1 presents the experimental scheme for the detection of the absorption spectrum of the nano-cell filled with Rb. It is important to note that the implemented $\lambda/2$ -method exploits strong narrowing of absorption spectrum at $L = \lambda/2$ as compared with the case of an ordinary cm-size cell [11, 14]. Particularly, the absorption line-width for Rb D_2 line ($L = \lambda/2 = 390 \text{ nm}$) reduces to about of 200 MHz (FWHM), as opposed to that in an ordinary cell (about of 500 MHz). In the experiment we used the radiation of a continuous wave narrowband diode laser with the wavelength of 780 nm and the width of 10 MHz. In the current experiment we had the choice to use a diode laser with the line-width of ≈ 1 MHz, however the mode hop free region is only of 5 GHz, which is too small to register all 20 atomic transitions. Meanwhile with the laser used in the experiment the mode hop free tuning range is 40 GHz. The linearity of the scanned frequency was tested by simultaneously recorded transmission spectra of a Fabry-Pérot etalon (not shown). The nonlinearity has been evaluated to be about 1% throughout the spectral range.

The strong magnetic field was produced by two $\varnothing 50$ mm permanent magnets (PM) with 3 mm holes (to allow the radiation to pass) placed on the opposite sides of the NTC oven and separated by a distance that

was varied between 40 and 25 mm (see the upper inset in Fig. 1). The magnetic field was measured by a calibrated Hall gauge. To control the magnetic field value, one of the magnets was mounted on a micrometric translation stage for longitudinal displacement. In the case where the minimum separation distance is of 25 mm, the magnetic field B produced inside the NTC reaches 3600 G. To enhance the magnetic field up to 6 kG, the two PM were fixed to a metallic magnetic core with a cross section of 40 mm x 50 mm. Additional form-wound Cu coils allow for the application of extra B -fields (up to ± 1 kG) (see the inset of Fig. 1).

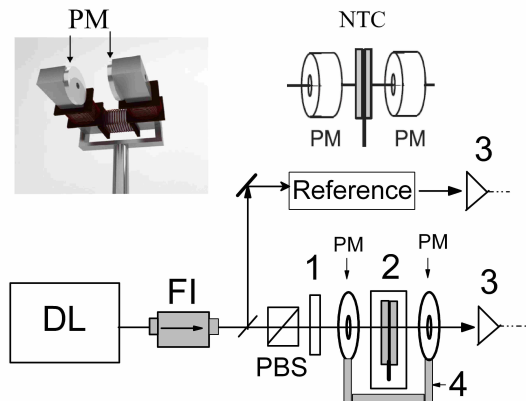


Figure 1: Sketch of the experimental setup. DL - tunable diode laser, FI - Faraday isolator, 1 - $\lambda/4$ plate, PBS - Polarizing Beam Splitter, 2 - NTC in the oven, Reference -(FR)- auxiliary Rb NTC providing $B = 0$ reference spectrum, PM - permanent magnets, 3 - photo-detectors, 4 - metallic magnetic core.

The beam with σ^+ circular polarization was formed by a $\lambda/4$ plate. The beam was focused by a lens ($F = 20$ cm) on the NTC to create a spot size ($1/e^2$ diameter, i.e. the distance where the power drops to 13.5 % of its peak value) in the cell of $d = 0.6$ mm and then collimated by a second lens (not shown in Fig. 1). To form the frequency reference (from which the frequency shifts were measured), a part of the laser beam was directed to a unit composed of an additional NTC with $L = \lambda/2$. The absorption spectrum of the latter at the atomic transition $F_g = 1 \rightarrow F_e = 1,2$ served as a reference (another weak transition $F_g = 1 \rightarrow F_e = 0$ is not well seen) [10].

3. EXPERIMENTAL RESULTS and DISCUSSIONS

3.1. Magnetic field $B < 3$ kG

In case of relatively low magnetic fields (~ 1 kG) there are 60 allowed Zeeman transitions when circular laser radiation excitation is used, with 22 atomic transitions belonging to ^{87}Rb , and 38 transitions belonging to ^{85}Rb D_2 line. These numerous atomic transitions are strongly overlapped and can be partially resolved

in case of using ^{87}Rb or ^{85}Rb isotope. When using natural Rb, the implementation of $\lambda/2$ -method allows one to resolve practically any individual atomic transition only for $B \geq 3$ kG.

The reduction of the total number of allowed atomic transitions at high magnetic fields down to 20 is caused by the effect of strong reduction of the atomic transitions probabilities for 40 transitions (such type of calculations for Rb D_1 line are presented in [19]). Note, that for $B \gg B_0$ the number of allowed transitions can be simply obtained from the diagrams shown in Fig. 4.

In Fig. 2 the absorption spectrum of Rb NTC with $L = \lambda/2$ for $B = 3550$ G and σ^+ laser excitation is

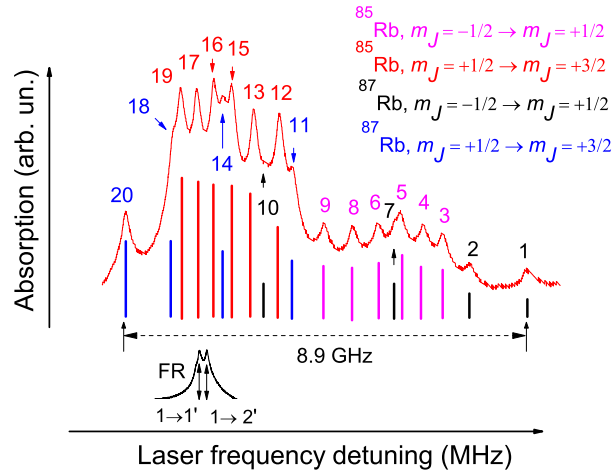


Figure 2: Absorption spectrum of Rb NTC with $L = \lambda/2$ for $B = 3550$ G and σ^+ laser excitation. The bottom curve (FR) is the absorption spectrum of the reference NTC showing the positions of ^{87}Rb $1 \rightarrow 1', 2'$ transitions for $B = 0$ (the frequency separation is 157 MHz). In the upper corner the corresponding atomic transitions are indicated. The absolute value of the peak absorption of the transition labeled as 1 is $\sim 0.3\%$.

shown. The laser power is $10 \mu\text{W}$. For Rb D_2 line there are 20 atomic absorption resonances located at the atomic transitions. Among these transitions 12 belong to ^{85}Rb , and 8 transitions belong to ^{87}Rb .

The atomic transition pairs labeled (19, 18) and (7, 5) are strongly overlapped (although in the case of strongly expanded spectrum the peaks belonging to the corresponding transitions are well detected), while the other 16 transitions are overlapped partially, and the positions of the absorption peaks are well seen. Thus, the fitting of the absorption spectrum with 20 atomic transitions is not a difficult problem. The vertical bars presented in Fig. 2 indicate the frequency positions and the magnitudes for individual transitions between the Zeeman sublevels as given by numerical simulations using the model described below. The corresponding atomic transitions presented by the vertical bars are indicated in the upper corner of Fig. 2.

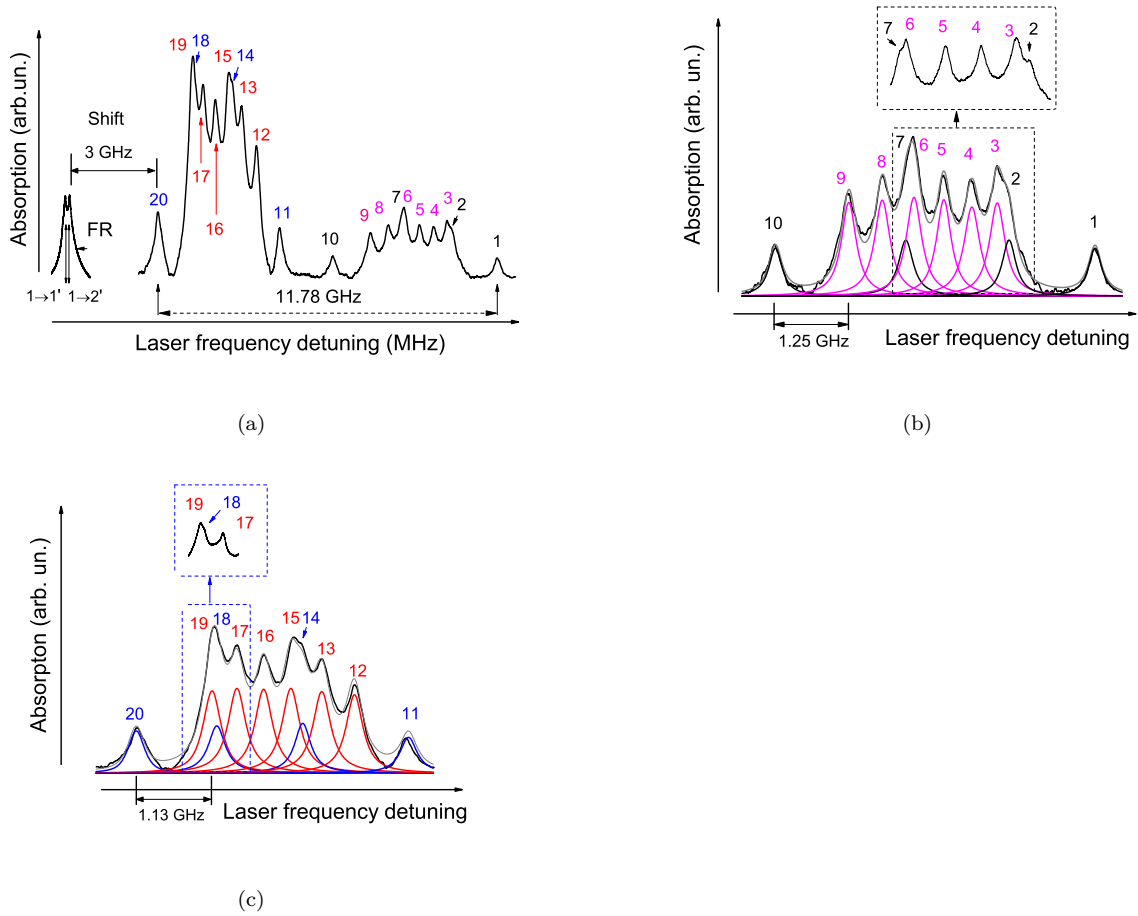


Figure 3: a) Absorption spectrum of Rb NTC with $L = \lambda/2$ for $B = 6850$ G and σ^+ laser excitation. For the transition labels, see Fig. 4. The left curve is the absorption spectrum of the reference NTC showing the positions of $^{87}\text{Rb } 1 \rightarrow 1', 2'$ transitions for $B = 0$ (the frequency separation is 157 MHz) and the frequency shift of the atomic transition labeled 20 with respect to $1 \rightarrow 2'$. b) The fragment of the absorption spectrum presented in Fig. 3(a). The group contains the atomic transitions labeled 1 – 10 which are fitted with the pseudo-Voigt profiles, with the line-width (Full Width Half Maximum) of 250 MHz; the inset shows an expanded view of the part of the experimental results limited by the dashed rectangle. c) The fragment of the absorption spectrum presented in Fig. 3(a) containing the atomic transitions labeled 11 – 20 which are fitted with the pseudo-Voigt profiles.

3.2. Magnetic field $B > 3$ kG : hyperfine Paschen-Back (HPB) regime

In case of strong ($B > 3$ kG) magnetic fields, the frequency separation between the atomic transitions increases, which allows one to separate practically any individual transition by using $\lambda/2$ -method. A remarkable value of the magnetic field is 4.5 kG, since at $B > 4.5$ kG, 20 atomic transitions are regrouped to form two separate groups of ten transitions each and the frequency interval between these two groups increases with the magnetic field (see below).

In Fig. 3 the absorption spectrum of Rb NTC of $L = \lambda/2$ for $B = 6850$ G and σ^+ laser excitation

is shown. There are still 20 atomic absorption resonances of Rb D_2 line located at the atomic transitions. Among these transitions, 12 belong to ^{85}Rb , and 8 transitions belong to ^{87}Rb . Atomic transition pairs labeled (19, 18), (15, 14) and (3, 2) are overlapped (although in the case of strongly expanded spectrum the peaks belonging to the corresponding transitions are well detected, see Fig. 3(c)) while the other 14 transitions are overlapped partially, and the positions of the absorption peaks of the individual transitions are well detected. The left curve presents the absorption spectrum of the reference NTC with $L = \lambda/2$ showing the positions of the ^{87}Rb , $F_g = 1 \rightarrow F_e = 1, 2$ transitions for $B = 0$ (the frequency shift of the transitions is determined with respect to $1 \rightarrow 2'$ transition).

Figure 3(b) shows the fragment of the spectrum (presented in Fig. 3(a)) for the atomic transitions labeled 1 – 10, where the transitions labeled 1, 2, 7 and 10 belong to ^{87}Rb , while the transitions labeled 3 – 6, 8, and 9 belong to ^{85}Rb . The fitting (with the pseudo-Voigt profiles [11]) is justified through the following advantageous property of the $\lambda/2$ -method: in case of a weak absorption, the absorption coefficient A of an individual transition component is proportional to σNL , where σ is the absorption cross-section proportional to d^2 (with d being the matrix element of the dipole moment), N is the atomic density, and L is the thickness. Measuring the ratio of A_i values for different individual transitions, it is straightforward to estimate their relative probabilities (line intensities).

The fragment of the spectrum (presented in Fig. 3(a)) is shown in Fig. 3(c) for the atomic transitions labeled 11 – 20, where the transitions labeled 11, 14, 18 and 20 belong to ^{87}Rb , while the transitions labeled 12, 13, 15, 16, 17, and 19 belong to ^{85}Rb .

It is important to note that, as seen from Fig. 3, the absorption peak numbered 1 is the most convenient for magnetic field measurements, since it is not overlapped with any other transition in the range of 1 – 10 kG (see also Fig. 4), while having a strong detuning value in the range of 2 – 2.3 MHz/G.

3.3. The manifestation of HPB regime.

The magnetic field required to decouple the electronic total angular momentum \mathbf{J} and the nuclear magnetic momentum \mathbf{I} is given by $B \gg B_0 = A_{hfs}/\mu_B$. For ^{85}Rb and ^{87}Rb it is estimated to be approximately equal to B_0 (^{87}Rb) ≈ 2 kG, and B_0 (^{85}Rb) ≈ 0.7 kG, where A_{hfs} is the ground-state hyperfine coupling coefficient for ^{87}Rb and ^{85}Rb and μ_B is the Bohr magneton [2, 16].

For such strong magnetic fields when \mathbf{I} and \mathbf{J} are decoupled (HPB regime), the eigenstates of the Hamiltonian are described in the uncoupled basis of J and I projections ($m_J; m_I$). Fig. 4(a) shows 12 atomic transitions of ^{85}Rb labeled 3 – 6, 8, 9, 12, 13, 15, 16, 17 and 19 for the case of σ^+ polarized laser excitation in the HPB regime and 8 transitions of ^{87}Rb labeled 1, 2, 7, 10, 11, 14, 18 and 20.

Simulations of magnetic sublevel energy and relative transition probabilities for Rb D_2 line are well known, and are based on the calculation of dependence of the eigenvalues and eigenvectors of the Hamilto-

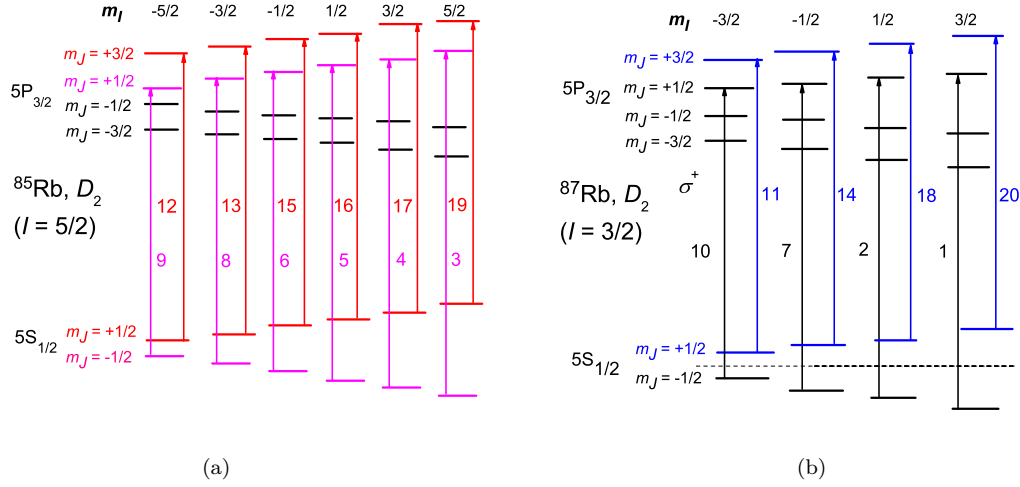


Figure 4: a) Diagram of ^{85}Rb , D_2 line ($I = 5/2$) transitions for σ^+ laser excitation in HPB regime. The selection rules: $\Delta m_J = +1$; $\Delta m_I = 0$. Therefore, there are 12 atomic transitions marked by the respective numbers 3 – 6, 8, 9, 12, 13, 15, 16, 17, and 19. b) Diagram of ^{87}Rb , D_2 line ($I = 3/2$) transitions for σ^+ laser excitation in HPB regime. Due to the selection rules there are 8 atomic transitions marked by the respective numbers 1, 2, 7, 10, 11, 14, 18, and 20.

nian matrix on magnetic field for the full hyperfine structure manifold [2, 4, 5, 17, 18, 19]. The calculated dependence of atomic transition probabilities (shown in Fig. 6) and frequency shifts vs B (shown in Fig. 5) are obtained using formulas (1)-(7) from work [11] and are omitted in the paper due to their bulkiness. Particularly, recently it has been demonstrated that the calculations using the above mentioned formulas perfectly well describe the experimental observation of a giant modification of the atomic probabilities of the Cs D_2 line $F_g = 3 \rightarrow F_e = 5$ transitions (which are forbidden for $B = 0$) in strong magnetic fields [20].

It is important to note that for $B \gg B_0$ the energy of the ground $5S_{1/2}$ and upper $5P_{3/2}$ levels for Rb D_2 line is given by the following equation [16]:

$$E_{|Jm_JIm_I\rangle} = A_{hfs}m_Jm_I + B_{hfs}\frac{3(m_Jm_I)^2 + \frac{3}{2}m_Jm_I - I(I+1)J(J+1)}{2J(2J-1)(2I-1)} + \mu_B(g_Jm_J + g_I m_I)B_z. \quad (1)$$

The values for nuclear (g_I) and fine structure (g_J) Landé factors and hyperfine constants A_{hfs} and B_{hfs} are given in [16]. Note, that Eq. (1) gives correct frequency positions of the components 1 – 20 with an inaccuracy of 2% practically when $B \geq 10B_0$, i.e. $B \geq 6 - 7$ kG for ^{85}Rb and $B \geq 20$ kG for ^{87}Rb [19].

Fig. 5 illustrates the frequency positions (i.e. frequency shifts) of the components 1 – 20 as functions of the magnetic field B . The theoretical curves are shown by solid lines. The black squares are the experimental results which are in a good agreement with the theoretical curves (with an error of 3%). As seen, the atomic transitions are regrouped at $B > 4500$ G to form two new sets of ten transitions each. Note, that the frequency separation between these two groups increases with B . The dashed line denotes the frequency position of the ^{87}Rb , $F_g = 1 \rightarrow F_e = 2$ transition for $B = 0$.

The experimental values of the slopes (the frequency shift with respect to the magnetic field) at

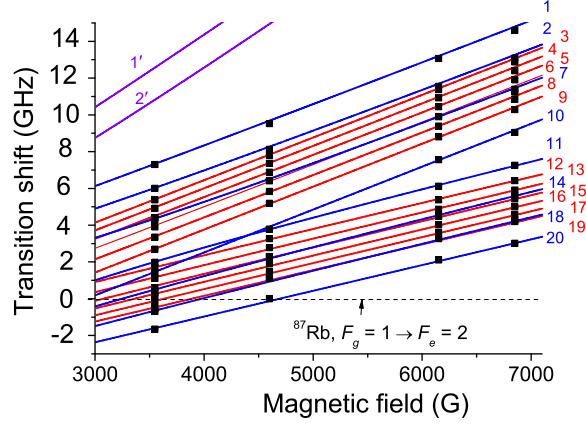


Figure 5: Frequency positions of the Rb, D_2 line atomic transitions 1 – 20 versus the magnetic field. Solid lines are the calculated curves and black squares are the experimental results (with an error of 3%). At $B > 4.5$ kG, the transitions are regrouped to form two groups of ten transitions each. For $B \gg B_0$ the frequency slope of the 1-st group (1 – 10 transitions) is $s_1 \approx 2.33$ MHz/G, and for the second group (11 – 20 transitions) $s_2 \approx 1.39$ MHz/G. Two upper curves show 1' and 2' belonging to the ^{87}Rb , D_2 , $F_g = 1 \rightarrow F_e = 3$ transitions, with the probability reducing to zero for $B > 6$ kG. Note, that magnetic field-induced strong modification of the probabilities for atomic transitions (which are forbidden by selection rules at $B = 0$) has been demonstrated in [18, 20].

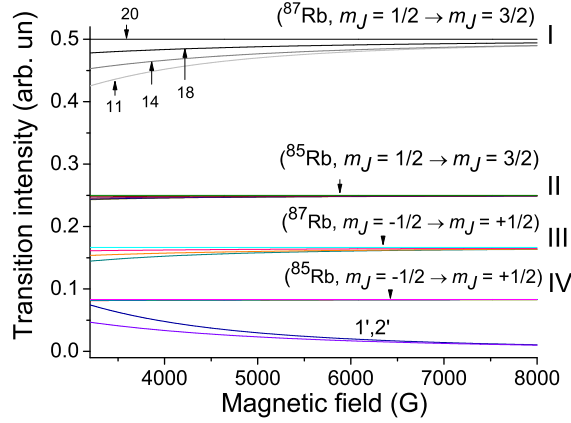


Figure 6: Intensity (probability) of the atomic transitions: (*I*-st group) ^{87}Rb , D_2 line transitions labeled 11, 14, 18, and 20; (*II*-nd group) ^{85}Rb , D_2 line transitions labeled 12, 13, 15 – 17, and 19; (*III*-rd group) ^{87}Rb , D_2 line transitions labeled 1, 2, 7, and 10; (*IV*-th group) ^{85}Rb , D_2 line transitions labeled 3, 4, 5, 6, 8 and 9. The transition probabilities differ significantly at low B -fields but tend to the same value within the group at $B \gg B_0$. Two lower curves show 1' and 2' belonging to the ^{87}Rb , D_2 , $F_g = 1 - F_e = 3$ transitions, with the probability reducing to zero for $B > 6$ kG.

$B = 7$ kG are $s_1 \approx 2.29$ MHz/G (for ^{85}Rb transitions this value is slightly larger, while for ^{87}Rb this value is slightly smaller) and $s_2 \approx 1.42$ MHz/G (for ^{85}Rb transitions this value is slightly smaller, while for ^{87}Rb this value is slightly larger) for the groups 1-10 and 11-20, respectively. It is noteworthy that the slope value for ^{87}Rb and ^{85}Rb (inside the same group, see Fig. 4) are nearly equal to each other when the initial and final energy levels are the same (see below).

The slopes of the transitions for the fields $B \gg B_0$ can be easily found from Eq. (1) as $s_1 = [g_J(P_{3/2})m_J - g_J(S_{1/2})m_J] \mu_B/B \approx 2.33$ MHz/G and $s_2 = [g_J(P_{3/2})m_J - g_J(S_{1/2})m_J] \mu_B/B \approx 1.39$ MHz/G for the groups 1 – 10 and 11 – 20, respectively (as $g_I \ll g_J$, we ignore $g_I m_I$ contribution). Consequently, at $B \geq 20$ kG (when the condition of HPB is fully satisfied for ^{87}Rb atoms, too), the slope for the group 1 – 10 increases slightly (to s_1), while the slope for the group 11 – 20 decreases slightly to s_2 . In addition, one can easily find from Eq. (1) the frequency intervals between the components within each group.

Figure 6 presents the theoretical values of “1 – 20” atomic transitions probabilities (intensities) in the fields of 5-7 kG. Let us compare the experimental results presented in Fig. 3 obtained for $B = 6850$ G with the theoretical calculations of the atomic transitions probabilities shown in Fig. 6. The atomic transitions labeled 3, 4, 5, 6, 8 and 9 of ^{85}Rb shown in Fig. 3(b) have the same amplitudes (probabilities) with inaccuracy less than 5% and this is in a good agreement with the theoretical curves shown in the IV-th group in Fig. 6. The atomic transitions labeled 12, 13, 15 – 17, and 19 shown in Fig. 3(c) have the same amplitudes (probabilities) with inaccuracy less than 5% and this is in a good agreement with the theoretical curves shown in the II-nd group in Fig. 6. It is easy to see that there is a similar good agreement between the amplitudes (probabilities) for the atomic transitions of ^{87}Rb shown in Fig. 3(b) and (c) with the theoretical curves shown in the I-st and III-rd groups presented in Fig. 6. Note, that the probabilities of the transitions for ^{87}Rb inside the same group 1-10 or 11-20 are nearly two times larger than the probabilities for ^{85}Rb inside the same group. However, since for natural rubidium the atomic density ratio $N(^{85}\text{Rb})/N(^{87}\text{Rb}) \approx 2.6$, the peak absorption of the atomic transitions for ^{85}Rb is nearly 1.5 times larger than that for ^{87}Rb (Fig. 6).

It is worth to note that the probability of the atomic transition for ^{87}Rb labeled 20 (for low magnetic field it could be presented as transition $F_g = 2, m_F = +2 \rightarrow F_e = 3, m_F = +3$) is the same in the whole range of magnetic field from zero up to 10 kG. This is caused by the absence of Zeeman sublevels with $F_g = 1, m_F = +2$ and $F_e = 2, m_F = +3$, since the perturbation induced by the magnetic field couples only sublevels with $\Delta m_F = 0$ which satisfies the selection rules $\Delta L = 0$, $\Delta J = 0$, $\Delta F = 1$, where L is the orbital angular momentum and F is the total atomic angular momentum (see formula (2) from [17]). Thus, probability modification is possible only for transitions between sublevels each of which is coupled with another transition according to the selection rules presented above. Due to the similar reason the probability of the atomic transition for ^{85}Rb labeled 19 (it could be presented as transition $F_g = 3, m_F = +3 \rightarrow F_e = 4, m_F = +4$) is also the same in the range of magnetic fields from zero up to 10 kG. Since for the transitions labeled 19 and 20 the absolute value of the probability could be calculated

from [16], thus using the experimental results presented in Fig. 3 the absolute value of the probabilities for the other atomic transitions (modified by magnetic field) can be calculated as well. Also, due to the above mentioned reason the frequency shifts of transitions labeled 19 and 20 as a function of magnetic field is simply linear with a fixed slope of $s = 1.39$ MHz/G. Note, that the reduction of the total number of Rb, D_2 transitions to strictly 20 in strong magnetic fields (which are well described by the diagrams presented in Fig. 4), as well as the behavior of the slopes s_1 and s_2 of ^{85}Rb and ^{87}Rb (which are close to the values obtained by Eq. 1) is the manifestation of the hyperfine Paschen-Back regime.

Note, that there are three main distinctions in the behavior of atomic transitions for D_2 line as compared with the behavior for D_1 line [5, 6].

i) At $B > 4.5$ kG in the absorption spectrum 20 well resolved atomic transitions are regrouped in two completely separate groups of 10 atomic transitions each and frequency separation between two groups increases with magnetic field. Meanwhile, for D_1 line there are only 10 atomic transitions forming one group.

ii) There are two remarkable atomic transitions for D_2 line: for ^{87}Rb atom, the transition labeled 20 and for ^{85}Rb atom, the transition labeled 19. In a wide region of magnetic fields from zero up to 10 kG the probabilities of these atomic transitions remain unchanged. Also, the frequency shifts of the transitions labeled 19 and 20 are simply linear versus magnetic B -field. Such type of remarkable atomic transitions is absent for D_1 line in the case of circular polarized laser radiation.

iii) In order to determine theoretically the frequency positions of atomic transitions in the case of D_1 line ($J = 1/2$) the well-known Rabi-Breit formulas can be implemented [16], while they are not useful for D_2 line ($J = 3/2$).

4. Conclusion

We present the results of experimental and theoretical studies of ^{87}Rb and ^{85}Rb D_2 line transitions in a wide range of magnetic fields $3 \text{ kG} < B < 7 \text{ kG}$. It is experimentally demonstrated that in the case of $B > 3$ kG and σ^+ polarized laser radiation, there remain only 20 Zeeman transitions while there are 60 allowed Zeeman transitions at low B -field. In the case of $B > 4.5$ kG in the absorption spectrum these 20 atomic transitions are regrouped to form two completely separate groups of 10 atomic transitions each with the frequency slopes s_1 and s_2 correspondingly. The frequency separation between the two groups increases with the magnetic field. The above mentioned peculiarities are the manifestation of hyperfine Paschen-Back regime. The implemented theoretical model very well describes the experiment.

Possible applications of the $\lambda/2$ -method can be mentioned: (i) making a reference at a strongly (up to ± 15 GHz) shifted frequency with respect to the initial atomic levels of Rb with the use of a permanent magnet as well as frequency locking of diode-laser radiation to these resonance [10]; (ii) designing a magnetometer

for measuring strongly inhomogeneous magnetic fields with a high spatial resolution [5]; (iii) designing an optical insulator based on Rb vapor with the use of the Faraday effect in strong magnetic fields (~ 6 kG), as was implemented in [7].

Taking into account that the probability of atomic transitions increases with B , we do not expect any limitations for using the $\lambda/2$ -method at $B > 10$ kG.

5. Acknowledgement

The research leading to these results has received funding from the European Union FP7/2007-2013 under grant agreement N° 295025-IPERA. The research was conducted in the scope of the International Associated Laboratory IRMAS (CNRS-France & SCS-Armenia). A.S., G.H., and D.S. acknowledge the support of the State Committee for Science, Ministry of Education and Science of the Republic of Armenia (project no. SCS 13-1C029).

References

- [1] P. Tremblay, A. Michaud, M. Levesque, S. Theriault, M. Breton, J. Beaubien and N. Cyr, Phys. Rev. A **42**, (1990) 2766–2773.
- [2] E. B. Alexandrov, M.P. Chaika, G.I. Khvostenko, *Interference of Atomic States* (Berlin; New York : Springer-Verlag, 1993).
- [3] D. Budker, W. Gawlik, D. Kimball, S.R. Rochester, V.V. Yaschuk, A. Weis, Rev. Mod. Phys. **74**, (2002) 1153-1201.
- [4] M. Auzinsh, D. Budker, S. M. Rochester, *Optically Polarized Atoms: Understanding Light-Atom Interactions* (Oxford University Press, ISBN 978-0-19-956512-2, 2010).
- [5] A. Sargsyan, G. Hakhumyan, A. Papoyan, D. Sarkisyan, A. Atvars, M. Auzinsh, Appl. Phys. Lett. **93**, (2008) 021119.
- [6] A. Sargsyan, G. Hakhumyan, C. Leroy, Y. Pashayan-Leroy, A. Papoyan, D. Sarkisyan, Opt. Lett. **37**, (2012) 1379.
- [7] L. Weller, K. S. Kleinbach, M. A. Zentile, S. Knappe, I. G. Hughes, and C. S. Adams, Opt. Lett. **37**, (2012) 3405.
- [8] L. Weller, K. S. Kleinbach, M. A. Zentile, S. Knappe, C. S. Adams and I.G. Hughes, J. Phys. B: At. Mol. Opt. Phys. **45**, (2012) 215005/7.
- [9] M. A. Zentile, R. Andrews, L. Weller, S. Knappe, C. S. Adams, and I.G. Hughes, J. Phys. B: At. Mol. Opt. Phys. **47**, (2014) 075005.
- [10] A. Sargsyan, A. Tonoyan, R. Mirzoyan, D. Sarkisyan, A.M. Wojciechowski, A. Stabrawa, and W. Gawlik, Opt. Lett. **39**, (2014) 2270.
- [11] A. Sargsyan, G. Hakhumyan, R. Mirzoyan, and D. Sarkisyan, JETP Letters **98**, (2013) 441.
- [12] C. Umfer, L. Windholz and M. Musso, Z. Phys. D – Atoms, Molecules and Clusters **25**, (1992) 23-29.
- [13] B. A. Olsen, B. Patton, Y.-Y. Jau, and W. Happer, Phys. Rev. A **84**, (2011) 063410.
- [14] D. Sarkisyan, D. Bloch, A. Papoyan, M. Ducloy, Opt. Commun. **200**, (2001) 201.
- [15] J. Keaveney, A. Sargsyan, U. Krohn, D. Sarkisyan, I.G. Hughes, C.S. Adams, Phys. Rev. Lett. **108**, (2012) 173601.
- [16] D. A. Steck, “Rubidium 85 D line data, Rubidium 87 D line data,” <http://steck.us/alkalidata>.
- [17] G. Hakhumyan, C. Leroy, Y. Pashayan-Leroy, D. Sarkisyan, M. Auzinsh, Opt. Commun., **284**, (2011) 4007.
- [18] G. Hakhumyan, C. Leroy, R. Mirzoyan, Y. Pashayan-Leroy and D. Sarkisyan, Eur. J. Phys. D **66**, (2012) 119.

- [19] A. Sargsyan, G. Hakhumyan, C. Leroy, Y. Pashayan-Leroy, A. Papoyan, D. Sarkisyan, and M. Auzinsh, *JOSA B* **31**, (2014) 1046.
- [20] A. Sargsyan, A. Tonoyan, G. Hakhumyan, A. Papoyan, E. Mariotti and D. Sarkisyan, *Laser Phys. Lett.* **11**, (2014) 055701.